Anal. Bioanal. Electrochem., Vol. 15, No. 7, 2023, 556-567
https://www.doi.org/10.22034/abec.2023.706509

Analytical & Bioanalytical Electrochemistry

Full Paper

Electrochemical Photodegradation of Methyl Red using Reduction Graphene Oxide of Palm Shells Supported TiO_2 Nanoparticle under Visible Irradiation

Irwan Irwan,[1] Intan Sari Jumbi,[2] Alimin Alimin,[2] Ratna Ratna,[3] Nohong Nohong,[2] Maulidiyah Maulidiyah,[2] Muh Nurdin,[2] and Muh Zakir Muzakkar[2,*]

[1]*Department of Pharmacy, Faculty of Sciences and Technology, Institut Teknologi dan Kesehatan Avicenna, Kendari 93117, Southeast Sulawesi, Indonesia*
[2]*Department of Chemistry, Faculty of Mathematics and Natural Sciences, Universitas Halu Oleo, Jl. H.E.A. Mokodompit Kampus Baru Anduonohu, Kendari 93232 – Southeast Sulawesi, Indonesia*
[3]*Chemistry Education Department, Teacher Training and Education Faculty, Universitas Halu Oleo, Kendari, Southeast Sulawesi 93232, Indonesia*

*Corresponding Author, Tel.: +6281341752784
E-Mail: zakir1703@yahoo.com

Received: 9 March 2023 / Received in revised form: 30 June 2023 / Accepted: 18 July 2023 / Published online: 31 July 2023

Abstract- Contamination of dyes such as methyl red in the aquatic environment causes numerous problems. Therefore, it is necessary to develop a novel catalyst that can quickly, accurately, and effectively eliminate dye contaminants. In this study, we report the successful preparation of a new candidate electrode, the rGOps-TiO_2 composite, via a hydrothermal method. Additionally, the electrodes were characterized using X-ray diffraction, spectroscopic techniques such as FTIR, and microscopic techniques such as SEM-EDX to ensure the synthesis of the prepared electrode material. The photocurrent response indicated that the rGOps-TiO_2 electrode exhibited higher visible light absorption compared to the undoped rGOps. The degradation efficiency of methyl red reached 90.04% in the UV irradiation-assisted photoelectrocatalytic process, which was significantly different from the efficiency achieved under visible light irradiation, which was 94.78%. Therefore, the photoelectrocatalytic (PEC) technique based on rGOps-TiO_2 showed much higher degradation efficiency for methyl red compared to the photocatalytic (PC) technique. This suggests that PEC holds promise for the treatment of dye wastewater in aquatic environments.

Keywords- Photoelectrocatalysis; rGOps-TiO_2 electrode; Methyl red; Synthetic dye; Catalytic degradation

1. INTRODUCTION

One of the reasons for environmental pollution is the presence of synthetic dye contamination. It is known that synthetic dyes are more stable, resistant to environmental conditions, brightly colored, and have a wide range of colors [1,2]. These dyes are thought to originate from various industrial activities such as coloring textiles, handicrafts, household appliances, vehicles, and building interiors [3]. Among the various synthetic dyes used, methyl red (MR) is the most frequently employed synthetic dye in the mentioned activities. MR, with the chemical name (2-(N,N-dimethyl-4-aminophenyl) azobenzenecarboxylic acid), belongs to the group of mono-azo dyes with a (—N=N—) bond. It is mutagenic and has a negative impact on human health [4,5]. Moreover, if inhaled or swallowed, it can cause skin irritation and affect the digestive tract [6]. Even worse, its effluents can cause severe environmental pollution even at low concentrations. This phenomenon has driven the need for efforts to control the various dyes that have been accumulating in the aquatic environment.

Recently, various conventional physical and chemical treatments have been attempted for the removal of synthetic dyes from wastewater, such as adsorption [7], coagulation [8], flocculation [9], zonation [10], and advanced oxidation process (AOP) technique [11]. Additionally, due to the chemical resistance of the azo group found in synthetic dyes, it is not easy to handle such wastewater through biological oxidation processes. Among the mentioned methods, the AOP technique has gained attention and favor in recent years due to its simplicity, low cost, and time efficiency [12]. Electrochemical photodegradation is a highly effective method for degrading poisonous organic compounds in wastewater. This process involves the use of photocatalytic degradable materials with the assistance of a natural or artificial light source. Particularly, it involves light irradiation by semiconductor oxides. Although many oxide semiconductor materials, such as ZnO, Bi_2O_3, NiO, WO_3, Cds, TiO_2, and others, have been investigated and reported [13]. TiO_2 nanoparticles are considered superior materials for a photocatalyst to remove toxic organic compounds. Moreover, TiO_2 is an n-type semiconductor with a band gap of 3.2 eV [14–16].

Although TiO_2 is considered a promising photocatalyst material, it still has drawbacks such as a wide bandgap energy and a high recombination rate of electron-hole pairs [17–20]. Therefore, to overcome these drawbacks and improve photodegradation efficiency, a supporting material is needed that can minimize the high rate of recombination and reduce the bandgap energy. Carbon-based materials such as carbon aerogel [21], carbon nanotube [22], carbon quantum dots [23], magnetic carbon [24], graphene oxide, rGO [25], and others have been investigated to enhance the photocatalytic efficiency of TiO_2 nanoparticles. In this study, TiO_2 nanoparticles are modified with reduced graphene oxide (rGO) to create binary nanocomposites. Additionally, owing to its negative charge density, rGO could facilitate cationic dye adsorption in an aqueous solution. Some researchers have reported that the modification of TiO_2 nanoparticles with rGO can lead to effective charge separation and

improved light absorption. Furthermore, rGO has been shown to enhance photocatalytic activity due to its high surface area and superior charge carriers [26].

In this work, we report a simple preparation method for the rGO/TiO_2 nanocomposite using the hydrothermal method. Previously, we performed rGO preparation. Actually, rGO can be obtained from various agricultural biomass wastes such as bagasse, sawdust, coconut shell, wood, palm shell, and more. However, rGO produced from palm shell waste is an interesting and highly promising material for catalyst-related applications, thanks to its high carbon content. Additionally, palm shell exhibits characteristics such as a porous surface area and high mechanical power. Palm shells are chosen as a precursor for graphene oxide due to their abundance and sustainability. Utilizing these shells as a precursor material aligns with the principles of green chemistry, emphasizing the use of renewable resources and minimizing waste. This approach aligns with the growing interest in developing environmentally friendly and economically viable methods for synthesizing graphene-based materials. Furthermore, in this work, we investigate the effects of UV irradiation and the mechanism of photocatalytic degradation of MR in an aqueous solution.

2. EXPERIMENTAL METHOD

2.1. Sample collection and preparation graphite powder

The palm shell was obtained from Kolaka Regency in Southeast Sulawesi, Indonesia. The raw material was cleaned, washed, and separated from the shell. It was then dried under the sun for 3-4 days. Afterward, the sample underwent carbonization to obtain high-carbon palm shell. Subsequently, the sample was mashed and sieved, resulting in a powder with a size of 200 mesh.

2.2. Nanocomposite electrodes synthesis and characterization

Graphene oxide from palm shells (rGOps) was synthesized using a modified Hummers' method [27]. In summary, 1.6 grams of rGOps and 100 mL of deionized water were placed in a hydrothermal reactor and heated at 160 ºC for 12 hours. Subsequently, it was dried in an oven at 105 ºC for 3 hours. The resulting rGOps powder was then calcined at 500 ºC for 1 hour. The crystal phase and structure of the synthesized nanocomposite were analyzed using X-ray diffraction (XRD). Additionally, the morphology and particle size were determined through Scanning Electron Microscopy (SEM), coupled with Energy-Dispersive X-ray Spectroscopy (EDX) to confirm the elemental content. The structure of the samples GOps, rGOps, and rGOps-TiO_2 had previously been confirmed using Fourier-transform infrared (FTIR) spectroscopy. Lastly, the nanocomposite's photocatalytic capability for degrading methyl red was examined using UV-Vis spectrophotometry.

2.3. Preparation of rGOps-TiO_2 nanocomposites working electrode

The body of the working electrode consists of a cylindrical glass with a 4 mm diameter, connected by a copper wire. In summary, the rGOps-TiO_2 composite was prepared by simply mixing TiO_2 Degussa P25 with varying masses (0.01 g, 0.05 g, and 0.1 g) with 0.7 g of rGOps. The mixture was then ground and sieved using a 200 mesh stainless steel sieve. Afterward, 0.3 g of paraffin oil was added and stirred for 30 minutes at a temperature of 80 °C. Prior to the experiment, the surface of the electrode was polished with paper until a smooth, shiny, and flat surface was achieved.

2.4. Photoelectrocatalytic degradation of methyl red dye

Photoelectrocatalytic degradation of methyl red dye was conducted over a three-electrode electrochemical system with Ag/AgCl as the reference electrode, Pt plate as the counter electrode, and rGOps-supported TiO_2 electrode as the working electrode (Figure 1). The system was operated using Multi-Pulse Amperometry (MPA) with a potential bias of 0.5 V, a 15-watt UV lamp with irradiation of 360 nm, and visible light of energy 18 Watts from a Xenon lamp. All these degradation experiments were evaluated in a photochemical reactor system at room temperature, taking MR of 2.0 mL each 10 min for 1 h. Subsequently, the degradation of methyl red was examined by using a UV-Vis spectrometer. Similar regard was conducted for the TiO_2 (as reference) electrode, with the same condition experiment.

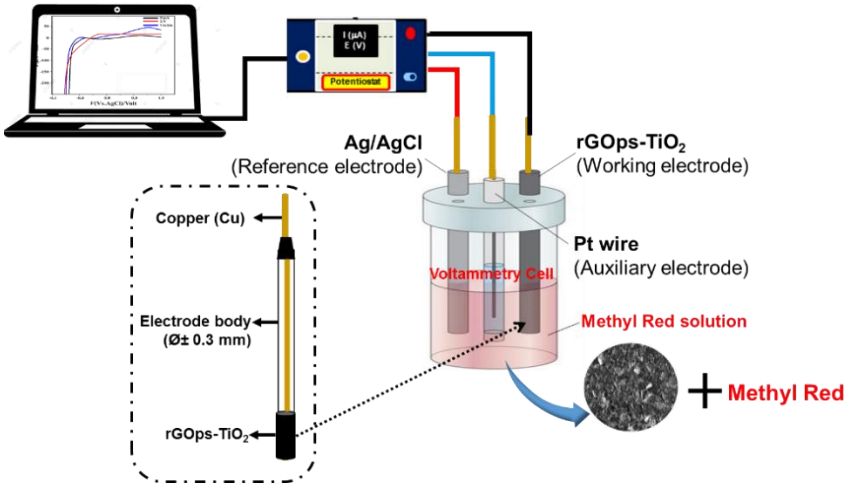

Figure 1. Illustration of working electrode body of rGOps-TiO_2 electrode by photo-electrochemical tests

3. RESULTS AND DISCUSSION

3.1. FTIR Analysis

Figure 2 displays the FT-IR spectra of the hydrothermally prepared rGOps-TiO_2 nanocomposite, reduced graphene oxide (rGO), and graphene oxide (GO). The FTIR spectrum

of the synthesized GO from palm shell reveals wide band peaks at 3423 cm^{-1}, attributed to O-H stretching. Additionally, other peaks at 2924 cm^{-1}, 1712 cm^{-1}, 1587 cm^{-1}, and 1028 cm^{-1} respectively, are associated with C-H stretching, C=O stretching, C=C stretching, and alkoxy C-O stretching. The presence of these peaks indicates the presence of graphene oxide, leading to the formation of reduced graphene oxide from palm shell (rGOps). Meanwhile, the IR spectrum of the rGOps-TiO_2 nanocomposite (Figure 2c) exhibits specific peaks at 1369 cm^{-1}, corresponding to the Ti-O bending, indicating the presence of TiO_2 nanoparticles in the nanocomposite [28,29]. This is further supported by X-ray Diffraction analysis data. Furthermore, the peak at 783 cm^{-1} correlates with the Ti-O-Ti functional group [30]. The wide peak observed at 3423 cm^{-1} confirms the O-H stretching vibration.

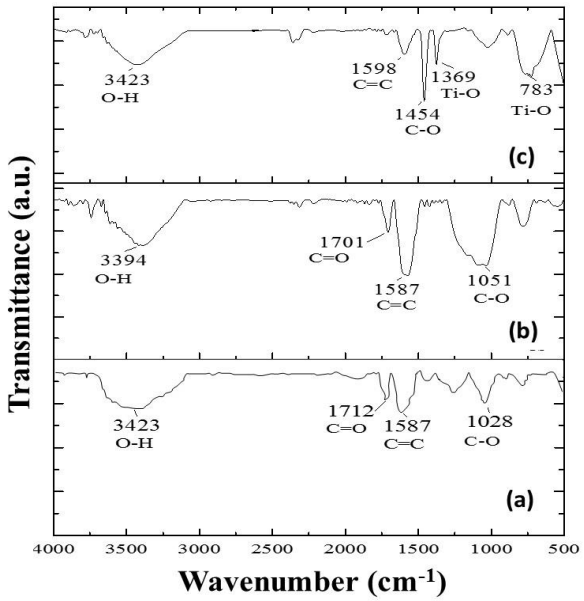

Figure 2. FTIR spectra of composite materials (a) GOps; (b) rGOps and (c) rGOps-TiO_2

3.2. SEM-EDX Analysis

The SEM images in Figure 3 display the rGOps and rGOps-TiO_2 nanocomposite produced through hydrothermal methods, with magnifications of 1,000x and 5,000x. A clear distinction can be observed between the two structures. The rGOps-TiO_2 nanocomposite exhibits an excessively porous structure in comparison to rGOps alone. Moreover, it is evident that the rGOps possess an uneven porous structure with a highly specific distribution [31]. The EDX spectrum analyses in Figure 3a indicate the presence of carbon (C) and oxygen (O) at 64.18 wt% and 29.55 wt%, respectively. Additionally, the rGOps-TiO_2 nanocomposite reveals a visibly rough porous structure, affirming the formation of TiO_2 nanoparticles on the surface of rGOps (Figure 3b). The EDX spectrum of rGOps-TiO_2 confirms the existence of titanium (Ti) content at 10.72 wt%, alongside other constituents such as carbon (C) and oxygen (O) at 50.44

wt% and 38.84 wt%, respectively (Figure 4b). These results support the effective distribution of TiO_2 nanoparticles on the rGOps surface.

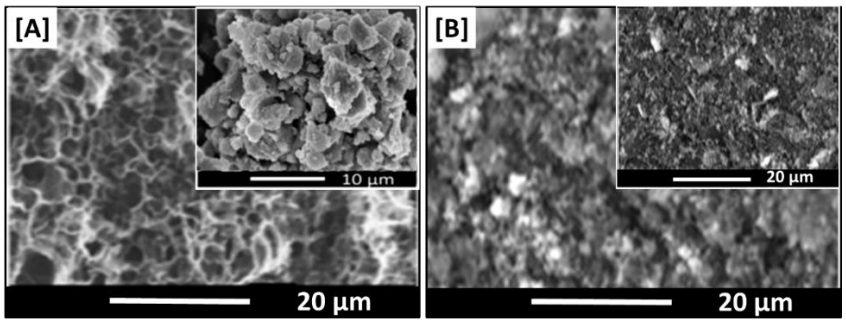

Figure 3. SEM image from (a) rGOps and (b) rGOps-TiO_2

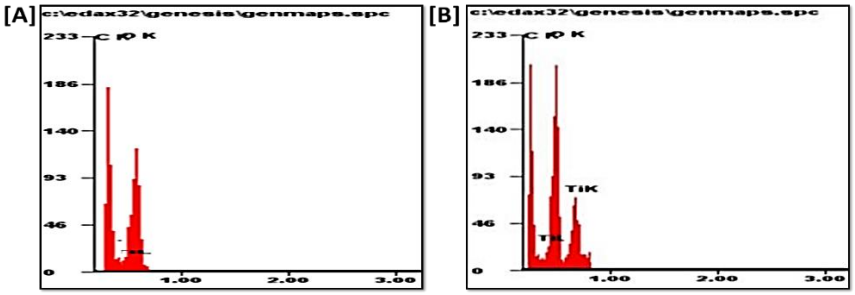

Figure 4. EDX spectra from (a) rGOps and (b) rGOps-TiO_2

3.3 XRD Analysis

The XRD patterns of rGOps and rGOps-TiO_2 are shown in Figure 5. Several peaks are visible at $2\theta =$ 25.24°, 37.8°, 44.04°, 53.88°, 54.17°, and 64.39°, corresponding to the crystallinity phases of TiO_2 in rGOps-TiO_2, which are suitable with Miller indexes (JCPDS file No. 00 021-1272) [32]. Additionally, there are two specific peaks at 25.24° and 44.04°, indicating the formation of anatase TiO_2 on the rGOps-TiO_2 surface. Other specific peaks observed around 37.8° and 54.17° correspond to the TiO_2 rutile phase [33]. The strong peaks in the XRD pattern of the prepared nanocomposite indicate the absence of impurities in the sample.

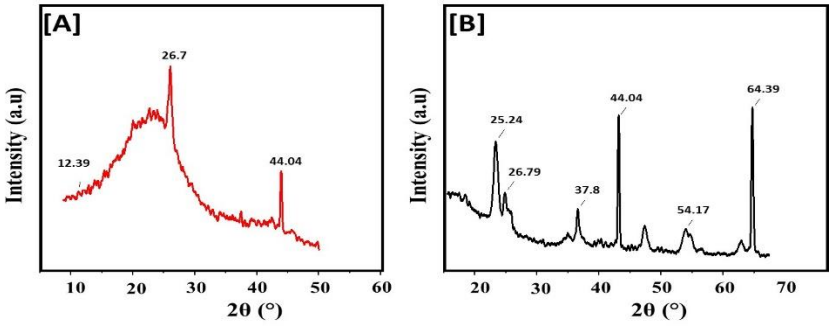

Figure 5. XRD pattern of (a) rGOps and (b) rGOps-TiO_2

3.4. Photoelectrocatalytic Performance

To evaluate the photoelectrocatalytic activity of rGOps and rGOps-TiO_2 electrodes, Linear Sweep Voltammetry (LSV) technique was employed. The experiment utilized rGOps and rGOps-TiO_2 as the working electrodes, Pt as the counter electrode, and Ag/AgCl as the reference electrode under UV-Vis irradiation. From the LSV graph shown in Fig. 4a, it is evident that the rGOps-TiO_2 nanocomposite electrode exhibited the highest current compared to the undoped rGOps. Furthermore, the rGOps-TiO_2 electrode demonstrated an increased current in the presence of visible light irradiation (Figure 4b). This phenomenon can be attributed to the enhanced mobility of electrons on the electrode surface, unlike the rGOps electrodes, which exhibited higher activity under UV irradiation [34]. The rGOps-TiO_2 electrode displayed the highest photocurrent response of 0.149 µA (under visible irradiation), while the undoped rGOps electrode yielded a photocurrent response of 0.15 µA. These results indicate that the rGOps-TiO_2 nanocomposite electrode was the most efficient and effective for degrading MR pollutants under visible light irradiation. To further confirm this, experiments using the Multi Pulse Amperometry (MPA) technique were conducted to assess the electrode's effectiveness [35].

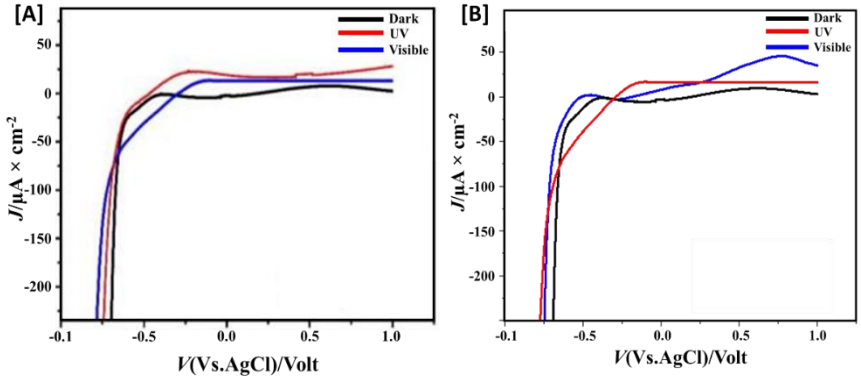

Figure 6. Linear Sweep Voltammetry (LSV) profile of rGOps Electrodes (A) and rGOps-TiO_2 (B) electrodes in 0.1 M solution $NaNO_3$ under UV and visible light irradiation

The electrochemical photodegradation performance of methyl red was examined using prepared electrodes under different conditions, including UV and visible irradiation. As shown in Figure 7, the degradation efficiency improved with increasing degradation time. It is evident that rGOps can only remove approximately 80.56% of MR in an aqueous solution under UV irradiation, whereas the rGOps-TiO_2 electrode can degrade about 90.04% of MR under the same conditions. Moreover, the rGOps-TiO_2 electrode achieved a degradation efficiency of 94.78% within 60 minutes with a concentration of 0.5 ppm (Figure 7B) under visible light irradiation, whereas the rGOps electrode achieved a degradation efficiency of approximately 61.61% (Figure 7a). This phenomenon demonstrates that TiO_2 nanoparticles supported on the

rGOps surface are more effective in discoloring MR compared to undoped rGOps during the photoelectrocatalytic reaction process. This can be attributed to the TiO_2-doped electrode having a higher current for the production of OH radicals, which are considered the primary contributors to the removal of organic pollutants on the rGOps-TiO_2 electrode. Furthermore, TiO_2 doping improves the surface area, thereby enhancing the contact time between the analyte and the electrode surface.

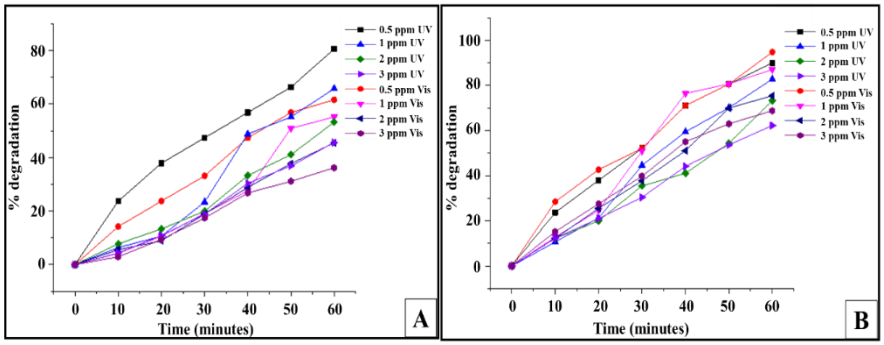

Figure 7. Photoelectrocatalytic degradation of methyl red compound using rGOps (A) and rGOps-TiO_2 (B) electrodes under UV and visible light irradiation

We further investigated the photocatalytic degradation of dye in the presence of rGOps and rGOps-TiO_2 photocatalysts under both UV and visible light irradiation. Figure 8 demonstrates that the rGOps-TiO_2 electrode exhibits significantly superior photocatalytic performance under visible light irradiation compared to UV light irradiation. The photocatalysts effectively degrade methyl red, achieving a degradation efficiency of up to 90%. In contrast, under UV irradiation conditions, only 80% degradation is achieved. As a comparative experiment, we also utilized the rGOps photocatalyst for the degradation of MR. However, the results were lower, with degradation efficiencies of only 75.82% under UV light irradiation and 85.30% under visible light irradiation.

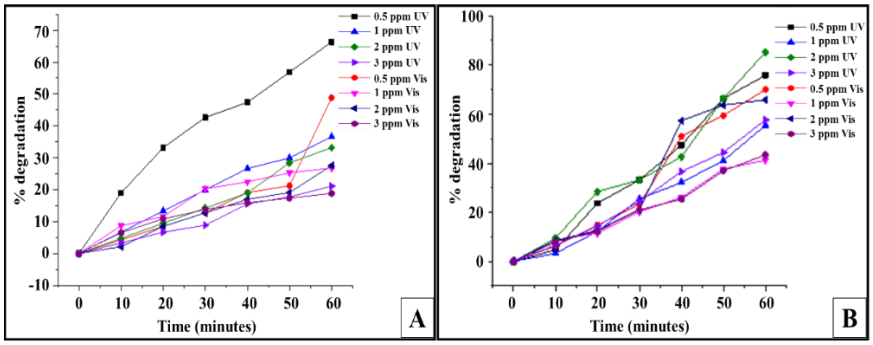

Figure 8. Photocatalytic degradation of methyl red over rGOps (A) and rGOps-TiO_2 (B) electrode under UV and visible light irradiation

Thus, based on these results, it is clear that the rGOps-TiO_2 electrode with a photoelectrocatalytic system demonstrates high activity under visible light irradiation. This is possibly due to the presence of TiO_2 nanoparticles on the surface of rGOps. In most cases, doping appears to improve the performance of the electrodes.

Therefore, photoelectrocatalysis systems based on rGOps-TiO_2 electrodes seem to be promising for the treatment of dye contaminants. In summary, the mechanism of photocatalytic degradation of MR in an aqueous solution using an rGOps-TiO_2 electrode is illustrated in Figure 9.

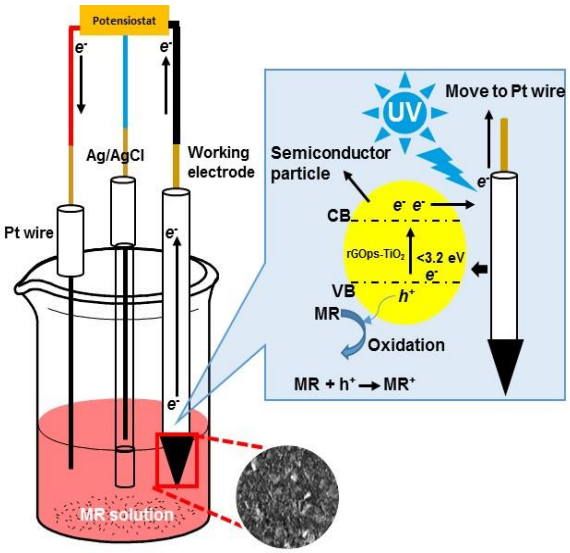

Figure 9. Illustration mechanism of photocatalytic degradation of MR in an aqueous solution using rGOps-TiO_2 electrode

The kinetics model for the degradation of MR was analyzed using either a first-order kinetic or the Langmuir-Hinshelwood (L-H) equation. This equation assists in the evaluation of the reaction rate constant by plotting ln C/C_0 against irradiation time (t) producing a straight-line curve with slope k'. From this curve, the degradation rate constant (K_d) is obtained which is presented in Table 1.

Table 1. The MR degradation rate constant for each concentration and the UV-visible lights irradiation of rGOps-TiO_2 by photocatalysis and Photoelectrocatalysis

Concentration (ppm)	**Photocatalytic Kd UV rGOps-TiO_2 (mg L^{-1} min^{-1})**	**Photocatalytic Kd Vis rGOps-TiO_2 (mg L^{-1} min^{-1})**	**Photoelectrocatalytic Kd UV rGOps-TiO_2 (mg L^{-1} min^{-1})**	**Photoelectrocatalytic Kd Vis rGOps-TiO_2 (mg L^{-1} min^{-1})**
0.5	0.024	0.028	0.0372	0.0434
1	0.0209	0.0207	0.029	0.0368
2	0.0131	0.014	0.0199	0.0242
3	0.0091	0.0094	0.0162	0.0201

Based on Table 1, it is evident that an increase in the solution concentration of thiamethoxam leads to a decrease in the degradation rate constant. This suggests that the photocatalysis and photoelectrocatalysis process was effectively progressing in the MR solution containing a low concentration. The reason behind this is that there was an equal quantity of catalyst present, resulting in a similar amount of the active surface side. Consequently, the MR solution when used at a lower concentration, would be fully taken in by the electrode's surface. This, in turn, led to a more effective photoelectrocatalytic process.

Moreover, numerous studies have previously documented a variety of comparisons involving the degradation of organic pollutants through photoelectrocatalytic processes, wherein TiO_2 photocatalysts were employed alongside different biomass waste precursors. These studies examined various concentrations of the pollutants, and their findings have been compiled and presented in Table 2.

Table 2. Comparison of contaminant degradation by photoelectrocatalytic process using TiO_2 photocatalyst with different biomass waste precursors

Precursor	**Type of Electrode**	**Contaminants**	**Concentration**	**Reference**
Coconut Shell	Graphene-TiO_2	Methylene Blue	10 mg L^{-1}	[36]
Bamboo Pulp Fibers	TiO_2-Carbon Aerogel	Methylene Blue	10 mg L^{-1}	[37]
Waste Walnut shells	TiO_2/Biochar	Methyl orange	5 mg L^{-1}	[38]
Palm Shell waste	rGOps-TiO_2	Methyl Red	0.5 - 3 mg L^{-1}	In this work

4. CONCLUSION

In summary, the rGOps-TiO_2 electrode was prepared using a hydrothermal method. The photoactivity examination under visible irradiation indicated that the rGOps-TiO_2 electrode can generate a higher current compared to the undoped rGOps. We also observed a linear correlation between the concentration of methyl red compounds and the current generated by the rGOps-TiO_2 electrode during the photoelectrocatalytic degradation process. Under UV conditions, the degradation percentage of methyl red was only 90.04% after 60 minutes of irradiation. However, under visible light irradiation, the rGOps-TiO_2 electrode was able to completely degrade methyl red, unlike the undoped rGOps electrode. This suggests that the rGOps-TiO_2 electrodes exhibit superior stability under visible irradiation. Additionally, the synergistic impact of photoelectrocatalysis significantly enhances the degradation and discoloration of methyl red compounds. Furthermore, we discovered that the PEC system is an effective method for the removal of dye wastewater.

Acknowledgments

We acknowledge the Titania Research Group and laboratory facilities support from the Department of Chemistry, Universitas Halu Oleo, Kendari, Indonesia.

Declarations of interest

The authors declare that there are no conflicts of interest in this article.

REFERENCES

[1] S.A.G.Z. Morsy, A. Tajudin, M.S.M. Ali, and F.M. Shariff, Front. Microbiol. 11 (2022) 572309.

[2] L.D. Ardila-Leal, R.A. Poutou-Piñales, A.M. Pedroza-Rodríguez, and B.E. Quevedo-Hidalgo, Molecules 26 (2021) 3813.

[3] G.A. Ismail, and H. Sakai, Chemosphere 291 (2022) 132906.

[4] P. Das, and A. Debnath, J. Dispers. Sci. Technol. (2022) 1, 10.1080/01932691.2022.2110110.

[5] M.N. Maniyam, A.L. Ibrahim, and A.E.G. Cass, Environ. Technol. 41 (2020) 71.

[6] M.V. Ratnam, C. Karthikeyan, K.N. Rao, and V. Meena, Mater. Today Proc. 26 (2020) 2308.

[7] T. Unugul, and F.U. Nigiz, Water, Air, Soil Pollut. 231 (2020) 1.

[8] W. Tianzhi, W. Weijie, H. Hongying, and S.T. Khu, J. Clean. Prod. 312 (2021) 127798.

[9] A. Karam, E.S. Bakhoum, and K. Zaher, Int. J. Sustain. Eng. 14 (2021) 983.

[10] K.G. Pavithra, and V. Jaikumar, J. Ind. Eng. Chem. 75 (2019) 1.

[11] P.V. Nidheesh, G. Divyapriya, F.E. Titchou, and M. Hamdani, Sep. Purif. Technol. 293 (2022) 121115.

[12] L. Zhu, J. Ji, J. Liu, S. Mine, M. Matsuoka, J. Zhang, and M. Xing, Angew. Chemie 132 (2020) 14072.

[13] A. Maurya, K.C. Majhi, and M. Yadav, Mater. Hydrog. Prod. Conversion, Storage (2023) 575.

[14] M. Nurdin, M.Z. Muzakkar, M. Maulidiyah, N. Maulidiyah, and D. Wibowo, J. Mater. Environ. Sci. 7 (2016) 3334.

[15] M. Nurdin, M. Maulidiyah, M.Z. Muzakkar, and A.A. Umar, Microchem. J. 145 (2019) 756.

[16] D. Wibowo, M.Z. Muzakkar, S.K.M. Saad, F. Mustapa, M. Maulidiyah, M. Nurdin, and A.A. Umar, J. Photochem. Photobiol. A 398 (2020) 112589.

[17] T. Azis, M. Maulidiyah, M.Z. Muzakkar, R. Ratna, S.W. Aziza, C.M. Bijang, O.A. Prabowo, D. Wibowo, and M. Nurdin, Surf. Eng. Appl. Electrochem. 57 (2021) 387.

[18] M. Nurdin, M.Z. Muzakkar, M. Maulidiyah, T. Trisna, Z. Arham, O.A. La Salim, I. Irwan, and A.A. Umar, Electrocatalysis (2022) 1.

[19] M. Maulidiyah, P.E. Susilowati, N.K. Mudhafardiyah, L.O.A. Salim, D. Wibowo, M.Z. Muzakkar, I. Irwan, Z. Arham, and M. Nurdin, Res. Appl. Chem. 12 (2022) 1628.

[20] M. Nurdin, L. Agusu, A.A.M Putra, M. Maulidiyah, Z. Arham, D. Wibowo, M.Z. Muzakkar, and A.A. Umar, J. Phys. Chem. Solids 131 (2019) 104.

[21] C.E.I. Torres, T.E.S. Quezada, O.V. Kharissova, B.I. Kharisov, and M.I.G. de la Fuente, J. Environ. Chem. Eng. 9 (2021) 104886.
[22] G. Rajakumar, X.H. Zhang, T. Gomathi, S.F. Wang, A.M. Ansari, G. Mydhili, G. Nirmala, M.A. Alzohairy, and I.M. Chung, Processes 8 (2020) 355.
[23] A. Alaghmandfard, O. Sedighi, N.T. Rezaei, A.A. Abedini, A.M. Khachatourian, M.S. Toprak, and A. Seifalian, Mater. Sci. Eng. C 120 (2021) 111756.
[24] H. Zhao, F. Wang, L. Cui, X. Xu, X. Han, and Y. Du, Nano-Micro Lett. 13 (2021) 1.
[25] P. Gholami, A. Khataee, R.D.C. Soltani, and A. Bhatnagar, Ultrason. Sonochem. 58 (2019) 104681.
[26] T.K. Le, M. Kang, and S.W. Kim, Mater. Sci. Semicond. Process. 100 (2019) 159.
[27] E.H. Sujiono, D. Zabrian, M.Y. Dahlan, B.D. Amin, and J. Agus, Heliyon 6 (2020) e04568.
[28] N. Ullah, S.M. Shah, R. Ansir, S. Erten-Ela, S. Mushtaq, and S. Zafar, Mater. Sci. Semicond. Process. 135 (2021) 106119.
[29] A. Ali, M. Shoeb, B. Li, and M.A. Khan, Mater. Sci. Semicond. Process. 150 (2022) 106974.
[30] E. Albiter, J.M. Barrera-Andrade, L.A. Calzada, J. García-Valdés, M.A. Valenzuela, and E. Rojas-García, Materials 15 (2022) 5284.
[31] L. Kong, X. Yin, H. Xu, X. Yuan, T. Wang, Z. Xu, J. Huang, R. Yang, and H. Fan, Carbon 145 (2019) 61.
[32] K.T. Drisya, M. Solís-López, J.J. Ríos-Ramírez, J.C. Durán-Álvarez, A. Rousseau, S. Velumani, R. Asomoza, A. Kassiba, A. Jantrania, and H. Castaneda, Sci. Rep. 10 (2020) 1.
[33] X. Xing, H. Zhu, M. Zhang, L. Xiao, Q. Li, and J. Yang, Chem. Phys. Lett. 727 (2019) 11.
[34] M. Nurdin, M.Z. Muzakkar, M. Maulidiyah, C. Sumarni, T. Azis, R. Ratna, M. Natsir, I. Irwan, L.O.A. Salim, and A.A. Umar, J. Appl. Electrochem. (2022)1.
[35] M.Z. Muzakkar, A.A. Umar, I. Ilham, Z. Saputra, L. Zulfikar, M. Maulidiyah, D. Wibowo, R. Ruslan, and M. Nurdin, J. Phys. Conf. Ser. (2019) 1242.
[36] A. Purabgola, N. Mayilswamy, and B. Kandasubramanian, Environ. Sci. Pollut. Res. 29 (2022) 32305.
[37] J. Zhang, W. Yuan, T. Xia, C. Ao, J. Zhao, B. Huang, Q. Wang, W. Zhang, and C. Lu Nanomaterials 11 (2021) 239.
[38] L. Lu, R. Shan, Y. Shi, S. Wang, and H. Yuan, Chemosphere 222 (2019) 391.